ACTA NEUROBIOLOGIAE EXPERIMENTALIS

Research paper Acta Neurobiol Exp 2009, 69: 504–525

Centroid extraction and illusions of extent with different contextual flanks

Aleksandr Bulatov[1]*, Algis Bertulis[1], Natalja Bulatova[1], and Yelena Loginovich[1]

[1]Institute of Biology, Kaunas University of Medicine, Kaunas, Lithuania, *Email: bulatov@vision.kmu.lt

In the present study, a computational model of the automatic centroid extraction based on the processes of local integration of excitatory profiles in the visual pathways has been developed. The model predictions have been compared with the results of our psychophysical examination of the perceptual distortions of the spatial extent. In experiments, the subjects matched two spatial intervals flanked by one of the three types of the contextual objects: either the Müller-Lyer wings, or vertical stripes, or spot pairs. A good resemblance between the theoretical functions and dependencies of the illusions' magnitudes on various spatial parameters of the stimuli has provided evidence that the effects caused by indirect positional coding *via* centroids are powerful enough to explain the phenomena of the geometric illusions investigated.

Key words: illusions of extent, contextual flanks, lateral interactions, centroid

INTRODUCTION

An early report on the illusion of linear extent was made by Baldwin (1895): the apparent length of a line was distorted by two flanking square boxes. Afterwards, Müller-Lyer (1896) invented his surprisingly simple figures flanked by arrowheads which later became widely known and often studied stimuli. Since then, numerous patterns with different contextual objects have been proposed to evoke the effects of illusions of extent, and the phenomena of illusions continue to be intensively used in investigations of mechanisms underlying the processing of sensory information. The accumulated data have shown that the contextual objects appended to stimuli influence its apparent size, but the strength of this influence depends on what the appendage is: the perceived metric properties of the illusory figures markedly depend on the structure, relative size, and relative location of the contextual flanks (Tausch 1954, Day 1972, Worrall and Firth 1974, Brigell et al. 1977, Gillam 1980, 1998).

One can take a view that the contextual flanks in the Müller-Lyer class of illusory figures may cause perceived mis-location of the terminators of the stimuli rather than a homogeneous compression or extension of the figure shaft as a whole (Mack et al. 1985). It is known that the eye movement system is programmed to produce saccades that end in the center-of-mass of figure elements surrounding the shaft end-point, that is, perceptual overestimation of the distance toward "wings-out" apices corresponds to an overshoot of saccades, while perceptual underestimation of the distance toward "wings-in" apices corresponds to an undershoot of saccades (Yarbus 1967, Festinger et al. 1968, Kaufman and Richards 1969, McLaughlin et al. 1969, Virsu 1971, Coren and Hoening 1972, Coren 1986). It has been shown that the inequalities of perceived length in the figure shaft divided into equal segments occurred only for the segments adjacent to the wings-shaft intersections (Morinaga 1941). A similar result was obtained in experiments with the distance markers placed at various positions along the shaft (Morgan et al. 1990). More recently, significant positional shifts in the shaft end-point were confirmed for the Müller-Lyer figure with the wings positioned on only one side of the shaft (Welch et al. 2004).

It has been established that the perceived locations of dots or thin lines correspond to the peaks of their light distributions (Chiang 1968, Glass 1970), while the experiments with more complex non-symmetrical

Correspondence should be addressed to A. Bulatov, Email: bulatov@vision.kmu.lt

Recived 22 April 2009, accepted 22 September 2009

objects revealed correspondence of their locations to the centroids, i.e., to averaged positions of the objects as wholes (Westheimer and McKee 1977, Watt and Morgan 1983, Morgan and Aiba 1985). The results of numerous studies of early visual processing confirm that the processes of lateral inhibition, neural noise, and blurring which occur in the visual pathways and have the effect of a certain spatial frequency filtering may cause significant averaging of the positional signals (Ward and Coren 1976, Ginsburg 1984, Morgan and Casco 1990, Earle and Maskell 1993, Bulatov et al. 1997, Fermüller and Malm 2004, Sierra-Vázquez and Serano-Pedraza 2007).

Efficient processing of visual information requires attentional selection of only a small fraction of the multitude of information presented to the visual system at any given time (Cavanagh and Alvarez 2005). A number of fMRI experiments have revealed significant enhancement of neural activation within a circumscribed regions of the cortical representations of the attended stimulus (Gandhi et al. 1999, Somers et al. 1999, Fink et al. 2002, Kelly et al. 2008). Neurophysiological single cell studies in behaving monkeys and lesion studies in both humans and primates have demonstrated the attentional modulation of the responses of individual neurons in almost all cortical areas, including V1 (Desimone and Duncan 1995). A wide variety of subcortical brain areas, such as midbrain superior colliculus or thalamus pulvinar, are also involved in different aspects of visual attention (Posner and Petersen 1990); e.g., neurons in the dorsomedial part of the pulvinar demonstrate strong enhancement in firing rate for attended stimuli within their receptive fields (Robinson and Peteresen 1992).

Visual selective attention can diverge from direction of gaze and be voluntarily focused on a peripheral part of the visual field. This allows, in particular, simultaneous tracking of multiple targets (Bettencourt and Somers 2009). However, so called "crowding" effect takes place, and even when attended items are easy to resolve visually, there are additional limitations of ability to select and identify individual items (Levi et al. 1985, Solomon et al. 2004). The psychophysical measurements of attentional resolution demonstrate that the size of the "spotlight of attention" is not homogeneous across the visual field and dramatically increases with the retinal eccentricity: from about 5 min of arc or less at the fovea center (Nakayama and Mackaben 1989, Toet and Levi 1992) to about 1.5º at 2º eccentricity (Sagi and Julesz 1986). Intriligator and Cavanagh (2001, p. 204) argued that attentional resolution "does not refer to the size of details being encoded, but to the spacing between details", and "will limit performance only when items are spaced more closely than the minimum required spacing for their particular spatial location".

In this way, illusions of extent may be a consequence of the limited ability of the visual system to extract the position of a part of an object independently of the immediately surrounding parts, and "objects composed of several different parts are located at the centroid of the individually measured positions of their parts" (Morgan et al. 1990, p. 1800). Averaging of the neural excitations evoked by the neighboring parts yields spatial pooling of the positional signals being conveyed to the high-level mechanism estimating the relative positions of objects in the visual field, which leads to the effect of indirect positional coding *via* centroids. Accordingly, the visual system is unable to evaluate accurately the distance between the certain elements belonging to the separate clusters of figural elements; instead, the distance perception is strongly affected by the positions of the centroids of the clusters as wholes. For example, in the Müller-Lyer and similar illusions, the visual system cannot successfully isolate the shaft end-points from the clusters of neighboring elements, and the judgments of the positions of the figure terminators are biased toward the positions of centroids of the corresponding contextual flanks.

An explanation of the Müller-Lyer illusion based on the idea of automatic centroid extraction (the concept of the centroid biases) was confirmed in psychophysical experiments with additional dots as non-target stimuli placed in various positions near the wings–shaft intersections (Searleman et al. 2005). The results demonstrated that the mechanism at work to produce the illusion is one that is locally applied at the wings intersections: the illusion magnitude was altered only when the extraneous dots were placed within a 2–3º radius around the figure shaft end-points (for shaft subtended about 9º). The conception of the centroid biases was successfully applied to the explanation of the experimental results with the Poggendorff (Morgan 1999), the Ponzo (Searleman et al. 2004), and the horizontal–vertical illusion (Searleman et al. 2003). Seizova-Cajic and Gillam's (2006) findings also support the interpretation for errors in judgments of spa-

tial separation in terms of centroid biases; however, this interpretation seems to fail to account for errors in judgments of orientation of imaginary lines connecting the elements belonging to different clusters.

Although a number of studies report their findings to be consistent with the concept of the centroid biases proposed by Morgan and others (1990), lack of detailed descriptions of mathematical and computational procedures of the mechanism of centroid extraction considered in these investigations does not allow evaluating quantitatively whether the effects of biases are powerful enough to explain illusion strength variations obtained experimentally with other illusory patterns. Therefore, in the present study, we develop a novel computational model of centroid extraction and test its theoretical predictions by performing a psychophysical examination of the illusions of extent with different types of contextual flanks. Recently, a similar approach was successfully applied to the explanation of influence of distracting flanks on the vernier alignment in a three-spot line arrangement and on the right angle perception (Bertulis et al. 2008).

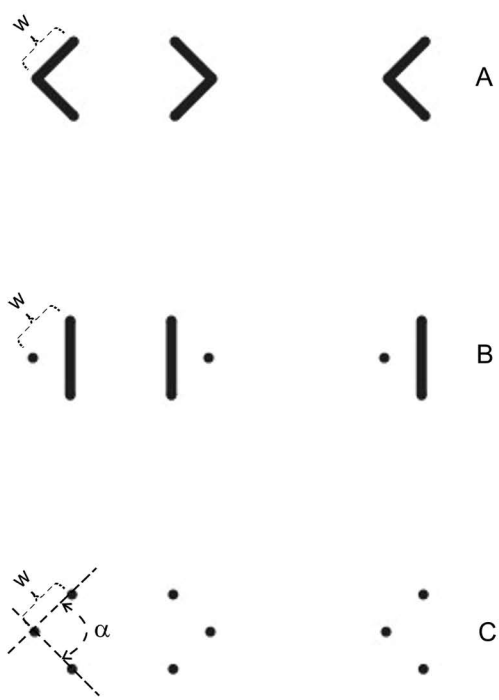

Fig. 1. Examples of the illusory stimuli used for the length matching task. Different contextual objects are present in the stimuli: (A) arrowheads made of two diagonal line segments, (B) vertical stripes, (C) vertically arranged pairs of spots. α – Internal angle of the wings, *w* – length of the wings; dashed lines – the dimensions were not part of the actual display.

In our psychophysical experiments, three types of flanking objects differing in the spatial structure but producing qualitatively similar perceptual distortions were used. One of the flanking objects was the Müller-Lyer wings displayed according to the Brentano pattern (Fig. 1A). The other type of flanking objects consisted just of vertical stripes integrated into the three-spot figure (Fig. 1B). Such a stimulus, which differs, at first sight, from the Brentano figure, was reported to induce the illusions of extent as regular functions of various stimulus parameters: the figure length, stripe height, contrast, and the size of gaps between the stripes and spots (Bulatov and Bertulis 2005b). And, the third illusory pattern used in our experiments (Fig. 1C), a modified Brentano figure, was made of nine separate elements which were common for both the patterns of Fig. 1A and Fig. 1B: the three pairs of flanking spots might be interpreted as the end-points of the imaginary Müller-Lyer wings, and, equally, they might be recognized as the end-points of the imaginary vertical stripes.

In the figures selected for the experiments, the shaft line was absent, and just three separate clusters comprising stimulus terminators and contextual flanks were present. All the clusters could be considered as imaginary triangles possessing different compound elements: in the figure with the Müller-Lyer wings, the triangles had two real diagonal sides, and an imaginary vertical one; in the illusory pattern with the flanking stripes, the triangles had a real vertical side but imaginary wings; and in the figure formed of spots, all sides of the triangles were imaginary. Therefore, the same independent variables were used: the length of the wings (the diagonal sides of the triangles), *w* in Experiments I and III; the internal angle, α between the wings in Experiment II. In addition, the stimulus size influence on the illusion strength was examined in Experiment III.

The main goal of our study was to develop a computational model based on the concept of centroid biases and compare the predictions of the model with the functional dependencies of perceptual distortions

established in the experiments. We concentrate on the idea that judgments of the distance between visual objects are affected by the automatic processes of centroid extraction, and leave other well known explanations of the origin of the illusions of extent beyond the limits of the study.

METHODS

At the beginning of this section, a certain physical and physiological background underlying procedure of the automatic centroid extraction is presented, followed by a detailed mathematical description of our modeling. Next, the experimental methods for measuring the strength of illusions of extent are described.

Modeling

The main idea of our modeling is based on the following physical statement: if mass M_a at $x = X$ is added to mass M at $x = 0$, the position of the centroid of the resulting system, τ is defined to be

$$\tau = \frac{XM_a}{M + M_a} = X\frac{m}{1+m} \qquad (1)$$

where the normalized mass, $m = M_a/M$. In the present approach, mass is considered as the amplitude of the neural excitation which is proportional to the object luminance, e.g., M and M_a are taken as luminance of the target (stimulus terminator) and distractor (contextual flank), respectively.

Let us first consider a simple hypothetical mechanism which allows extraction of the centroid position, τ, on the arbitrary x-axis. The mechanism can be assembled from the evenly distributed summation units (Fig. 2A, left) which possess a linear weighting profile along the x-axis, and a constant one along the orthogonal y-axis, $L(x,y)$:

$$L(x,y) = -kx \cdot \Phi\left(x, y, D_x, D_y\right) \qquad (2)$$

where k is a scale coefficient; $\Phi(x,y,D_x,D_y)$ is the zero-centered window with the constant weighting profile; and D_x *and* D_y are the dimensions of the window along the x and y axes, respectively. Obviously, the window should be at least two times larger than the extent of the pattern of masses considered, i.e., $D_x \geq 2X$.

Convolution of the weighting profile $L(x,y)$ with the function of the distribution of masses yields the centroid position on x-axis under condition of the equilibrium:

$$\begin{aligned}&\int\int_{\infty} L(\tau - x, y)\{\delta(x)\delta(y) + \\ &+ m\delta(x - X)\delta(y)\}dxdy = \\ &= L(\tau, 0) + mL(\tau - X, 0) = 0\end{aligned} \qquad (3)$$

Then,

$$k\tau = km(X - \tau), \text{ or } \tau = X\frac{m}{1+m}$$

where τ is the resulting centroid position which corresponds to that of the summation unit with the balanced zero response (Fig. 2A, right); for simplicity, but without loss of generality, we use lumped distribution of masses described by the Dirac delta functions $\delta(x)$ $\delta(y)$ and $m\delta(x–X)\delta(y)$ for the target and distractor, respectively. Analogically, position of the centroid on the other axis of the pattern can be obtained by using the system of the summation units oriented correspondingly.

Although the mechanism described is convenient for the straightforward illustration of the principle of centroid extraction, another, equivalent scheme seems to be more adequate: the summation units of the mechanism have, instead of linear, the parabolic (Fig. 2B, left) type of the weighting profile, $Q(x,y)$:

$$Q(x,y) = \left(1 - \frac{k}{2}x^2\right) \cdot \Phi\left(x, y, D_x, D_y\right) \qquad (4)$$

In this case, the centroid position corresponds to the position of the summation unit with the maximum response (Fig. 2B, center); analytically, the position of maximum is also determined by Equation 3, because $L(x,y)$ corresponds to the first derivative of $Q(x,y)$.

In the visual system, the summation units with receptive fields possessing the parabolic (or linear) and the constant weighting profiles in mutually orthogonal directions are, presumably, absent. Instead, the receptive fields with weighting profiles as a combination of properly aligned subfields (like in case of thalamic input to simple cells of primary visual cortex) each of which possesses the profile of the circular Gaussian, or the Difference-of-

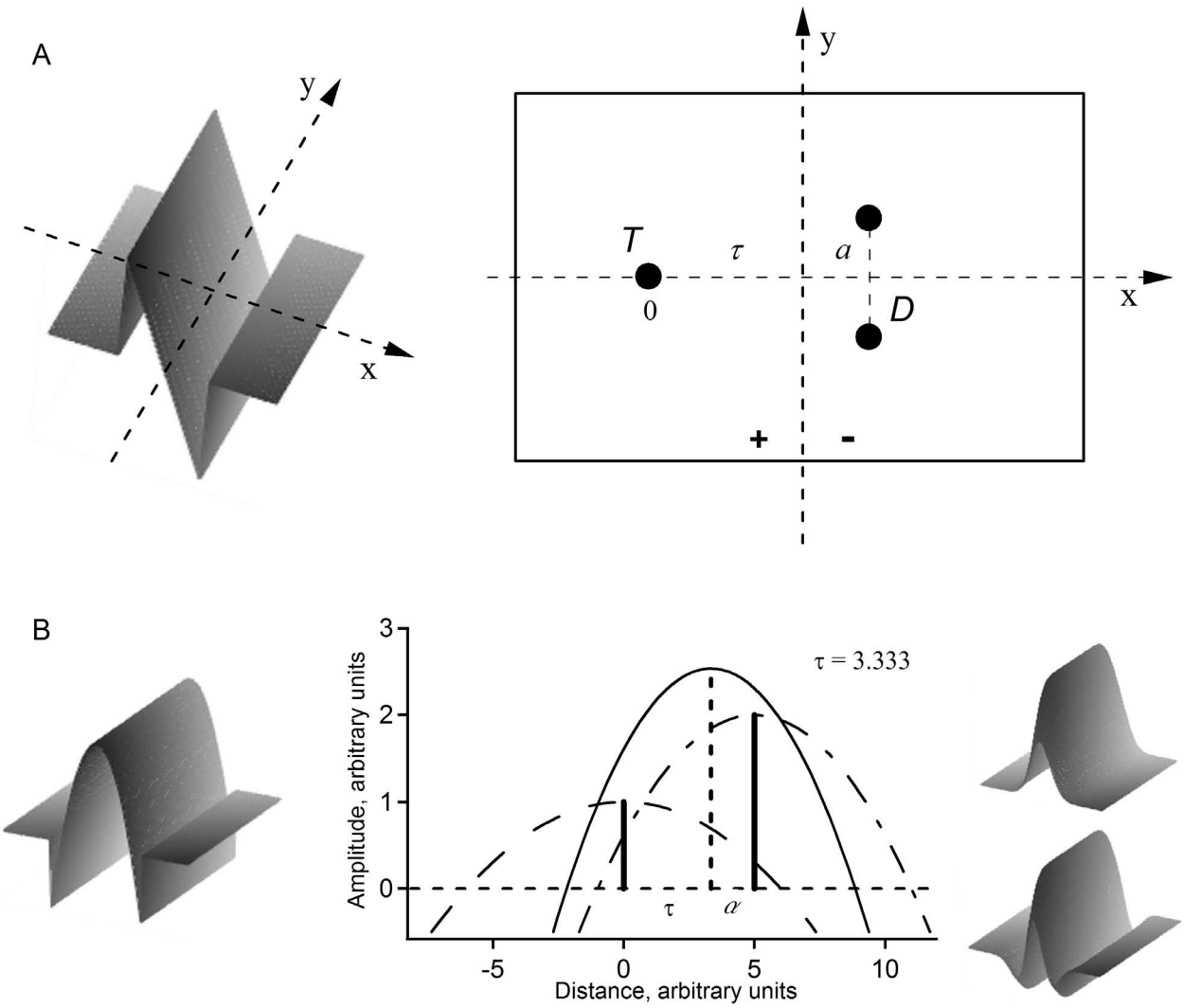

Fig. 2. Diagrams illustrating the mechanism of centroid extraction. (A) Left – two-dimensional view of the weighting profile of the summation unit, $L(x,y)$ represented by linear and constant functions in mutually orthogonal axes x and y; right – determination of the centroid location on the x axis: +/− represents positive and negative halves of the linear weighting profile windowed by a rectangle; $x = 0$, the position of the terminator, T the mass of which is m; $x = X = \tau + a$, the position of the distractor, D (comprising two spots) the mass of which is $2m$; $x = \tau$, the centroid position corresponding to the position of the summation unit with the balanced zero response, $m \cdot \tau - 2m \cdot a = 0$. (B) Left – two-dimensional view of the weighting profile of the summation unit, $Q(x,y)$ represented by parabolic and constant functions in mutually orthogonal axes x and y; center, one-dimensional view of determination of the centroid location: $x = 0$, the position of the terminator (left vertical bar) the mass of which is 1; $x = \tau + a = 5$, the position of the distractor (right vertical bar) the mass of which is 2; dashed curve represents the result of convolution of the summation unit profile and the terminator mass distribution in the distractor absence; dashed-dotted curve shows the result of convolution of the summation unit profile and the distractor mass distribution in the terminator absence; solid curve represents the result of convolution in the presence of both the terminator and distractor; the centroid position, $x = \tau$ corresponds to the position of the curve maximum coinciding with the position of the summation unit with the maximum response (vertical dashed line); right – two-dimensional view of the weighting profiles of the summation units represented by Gaussian (upper) and Laplacian-of-Gaussian (lower) functions.

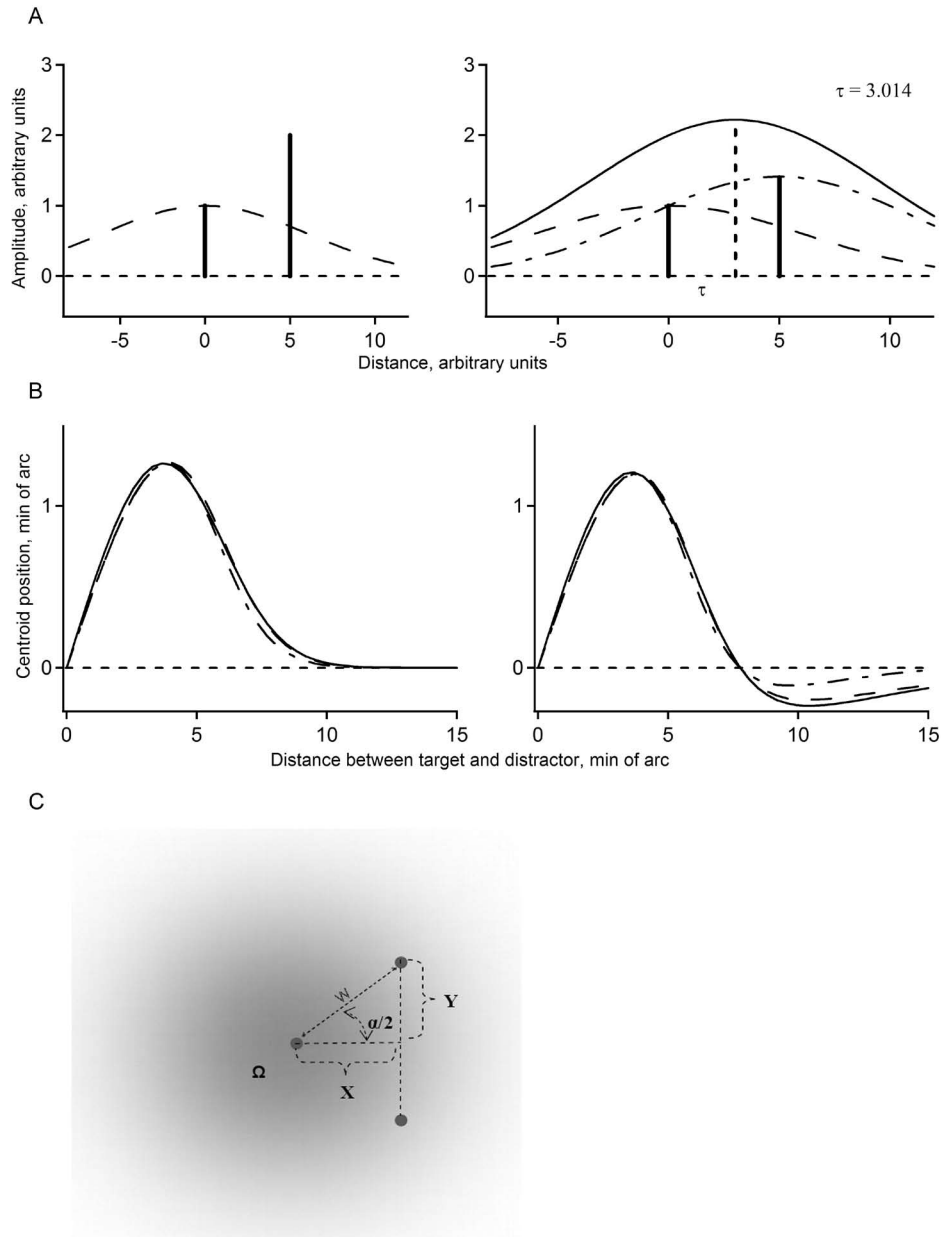

Fig. 3. Diagrams illustrating the modeling. (A) Left – one-dimensional view of the initial distribution of masses of the terminator and distractor with the ratio 1:2 (vertical bars); dashed curve shows the weighting profile of the attentional pooling window; right, one-dimensional view of determination of the centroid location: vertical bars show the terminator and distractor masses after the pooling procedure; dashed curve represents the result of convolution of the Gaussian profile of the summation unit and the terminator mass distribution in the distractor absence; dashed-dotted curve shows the result of convolution of the summation unit profile and the distractor mass distribution in the terminator absence; solid curve represents the result of convolution in the presence of both the terminator and distractor; the centroid position, $x = \tau$ corresponds to the position of the curve maximum coinciding with the position of the summation unit with the maximum response (vertical dashed line). (B) Calculated centroid position as a function of the distance between the target and distractor with their mass ratio 1:2 for the weighting profile of the attentional pooling window of the Gaussian type (left) and Laplacian-of-Gaussian type (right); the results of the exact root-finding are represented by the dashed and dashed-dotted curves for the Gaussian and Laplacian-of-Gaussian weighting profiles of the summation units, respectively; the data obtained by the approximate Formula 5 are shown by the solid curves. (C) Ω – the attentional pooling area centered with the stimulus terminator spot; w – length of the wings, α – internal angle of the wings, $X = w\cos(0.5\alpha)$, and $Y = w\sin(0.5\alpha)$.

Gaussian (DoG), or the Laplacian-of-Gaussian (LoG), are widely presented (Fig. 2B, right). The profiles resemble, at first approximation, properties of quadratic parabola (e.g., LoG function can be directly considered as the parabola windowed by Gaussian) and might be used as appropriate weighting functions in the summation units of the mechanism of centroid extraction.

Considering the local character of averaging of the positional signals, we assume that the procedure of a weighted attentional pooling over proximal surroundings of each stimulus terminator occurs: the relief of the neural excitation evoked by the stimulus terminator and contextual flanks is multiplied by the circular Gaussian (or DoG, or LoG) profile of a hypothetical pooling window. As a result, the procedure of the attentional pooling increases actual ratio of masses (terminator/flank) and attenuates the influence of more distant elements in a cluster. Figure 3A provides an illustration of consequent procedures of modeling.

Substitution of the linear function $L(x,y)$ in Equation 3 by the first derivative of Gaussian (or that of DoG, or LoG), $F'(x,y)$ yields the formula

$$\iint_{\infty} F'(\tau - x, y)e^{-P(x^2+y^2)}\{\delta(x)\delta(y) + m\delta(x - X)\delta(y)\}dxdy = 0$$

which is not amenable to an exact analytical solution, and only numerical root-finding is possible (here, parameter P determines the width of the Gaussian of the pooling window). Therefore, we take Gaussian function for the weighting profile of the summation unit as one of the simplest and assume that the centroid position can be estimated by the approximate formula:

$$\tau \cong X\frac{me^{-PX^2}}{1+me^{-PX^2}}e^{-SX^2\left(\frac{1-me^{-PX^2}}{1+me^{-PX^2}}\right)} \approx \approx X\frac{me^{-PX^2}}{1+me^{-PX^2}}e^{-SX^2} \quad (5)$$

where τ is the resulting centroid position; X is the distance between the target and distractor; the parameters P and S determine the widths of the Gaussians of the pooling and summation units, respectively. Goodness of approximation of the results of numerical root-finding by Formula 5 is illustrated in Fig. 3B. Generally, for the reliable centroid extraction (i.e., to escape the multiple maxima in a resulting excitation profile), the width of the summation unit should not be smaller than the diameter of the pooling window. Therefore, the spatial limits of the local integration of positional signals are determined mainly by the size and the position of the attentional pooling window. We define the local complex of the pooling window and the receptive fields of the summation units as the area of centroid extraction, Ω.

In our calculations, we consider a single part of the illusory figure 1C which is composed of three spots and assume that the area of centroid extraction Ω is centered with the terminator spot (Fig. 3C). To simplify calculations, we assume that the excitation profile consists of three cylinders, widths of which are equal to the spot diameter s, and the heights (excitation amplitudes) are equal to 1. Multiplication of two profiles, the excitation and the pooling window, shows that the mass corresponding to the terminator spot can be written as:

$$M = \int_0^{2\pi}\left(\int_0^{0.5s}\rho e^{-B\rho^2}d\rho\right)d\varphi = = \frac{\pi}{B}\left(1-e^{-0.25Bs^2}\right) \cong \frac{\pi}{B}erf\left(0.5s\sqrt{B}\right)^2$$

where erf(x) is the error function encountered in integrating the normal distribution; $B=0.5\sigma^{-2}$, where σ determines the width of the Gaussian profile of the pooling window.

Then, the mass corresponding to the contextual flank comprising two spots can be written as:

$$m_{dd} \approx 2Me^{-B(X^2+Y^2)} = 2Me^{-Bw^2}$$

where w is the wing length, α is internal angle; $X = w\cos(0.5\alpha)$, and $Y = w\sin(0.5\alpha)$.

If we suppose, for simplicity, the same σ's for the pooling window and summation units in Formula 5, the centroid position (which corresponds to the perceived position of a single terminator spot) can be modeled as follows:

$$\tau_{dd} = X\frac{m_{dd}}{M+m_{dd}}e^{-BX^2} = = X\frac{2e^{-Bw^2}}{1+2e^{-Bw^2}}e^{-BX^2} \quad (6)$$

The analogous calculations can be applied to the other illusory figures. Integrating along the vertical line, the length of which is $2Y$ and the width is s, yields the mass corresponding to the contextual stripe:

$$m_{ds} = e^{-BX^2}\sqrt{\frac{\pi}{B}}erf\left(0.5s\sqrt{B}\right)\int_{-Y}^{Y}e^{-BY^2}dy =$$

$$= \frac{\pi}{B}e^{-BX^2}erf\left(Y\sqrt{B}\right)erf\left(0.5s\sqrt{B}\right)$$

Then, the centroid position which corresponds to the perceived position of the terminator spot (Fig. 1B) is:

$$\tau_{dd} = X\frac{m_{ds}}{M + m_{ds}}e^{-BX^2} =$$

$$= X\frac{e^{-2BX^2}erf\left(Y\sqrt{B}\right)}{erf\left(0.5s\sqrt{B}\right) + e^{-BX^2}erf\left(Y\sqrt{B}\right)}e^{-BX^2} \quad (7)$$

For stimulus in Fig. 1A, the x projection of the local mass of the Müller-Lyer wings is:

$$m_{ml}(x) = \frac{2}{\cos(0.5\alpha)}e^{-B\left[\frac{x}{\cos(0.5\alpha)}\right]^2}\times$$

$$\times\sqrt{\frac{\pi}{B}}erf\left(0.5s\sqrt{B}\right)$$

Integrating along x axis gives the resulting centroid position:

$$\tau_{ml} = \frac{\int_0^X xe^{-Bx^2}m_{ml}(x)dx}{\int_0^X m_{ml}(x)dx} =$$

$$= X\frac{1 - e^{-Bw^2\left[1+\cos(0.5\alpha)^2\right]}}{\left[1 + \cos(0.5\alpha)^2\right]w\sqrt{\pi B}erf\left(w\sqrt{B}\right)} \quad (8)$$

Evidently, the proposed principle of calculations of centroid extraction can be easily applied to some other illusory patterns with different spatial structure.

It should be noted that the present modeling is not concerned with the 2D spatial frequency filtering which takes place at the early stages of the visual processing (Bulatov et al. 1997, Bulatov and Bertulis 2005a). Due to filtering (which possesses some properties of 2D second derivative), the regions of the endpoints and line crossings in the stimulus excitation patterns can be emphasized because of a higher degree of spatial discontinuity. In our study, the filtering can strengthen the similarity of the excitation profiles evoked by different contextual objects consisting of line segments or spots.

Next, we present the methods of psychophysical experiments whose results are to be compared with the predictions of our model.

Apparatus

The experiments were carried out in a dark room. A Sony SDM-HS95P monitor was used for the stimuli presentations. A Cambridge Research Systems OptiCAL photometer was applied for the monitor luminance range calibration and gamma correction. A chin holder and an artificial pupil with 3 mm diameter were used. The distance between the subject's eye and the screen was 400 cm. The right eye was always tested irrespective of whether or not it was the leading eye. The experiments were conducted under control of computer software of our design arranging the order of the stimuli, presenting them on the monitor, introducing alterations according to the subject's command, recording the subject's responses, and handling the results. The Microsoft GDI+ antialiasing technique was applied for the stimuli drawings.

Stimuli

The stimuli were arranged horizontally and presented monocularly against a round-shaped background of 4° in diameter and 0.4 cd/m^2 in luminance. The stimulus luminance was 75 cd/m^2. The spots of the stimuli were 1.5 min of arc in diameter, and the lines of the wings and stripes were 1.5 min of arc thick. The central spot of the stimuli or the vertex of the middle wings of the Brentano figure were always present in the center of the background. The left interval of the stimuli (spatial interval between the left and the central spots or vertices) was considered the referential part, and the right interval the test one.

Procedure

To establish functional dependence of the illusion strength on the spatial parameters of the stimuli, we used the method of adjustment. Biases of the judgment criteria which are an inherent characteristic of the method were reduced by randomizing both stimuli of different types and values of the independent variables in the presentation sequence. Regardless of the relative roughness, the method of adjustment provides collecting the data sufficient for estimation of the shapes of the experimental curves and for speculations concerning the illusions' nature.

The subjects were asked to manipulate the keyboard buttons to change the length of the test interval by adjusting its end-spot into a position that makes the test interval to appear equal to the perceived length of the referential interval. A single button push varied the size of the test interval by one pixel corresponding approximately to 0.25 min of arc. The initial length of the test interval of the stimulus was randomized: the length differences between the test and the referential intervals were distributed evenly within a range of ± 5 min of arc. The subjects did not know in advance whether the computer program would show a longer or shorter test interval than the referential one. When the subject varied the test interval length, the wing length and tilt angle of the Brentano stimuli remained unchanged, also the stripe height and spot-to-stripe gap of the stimuli with the flanking stripes remained constant in size. In Experiments I, II, and in the first series of Experiment III the subjects were given no instructions concerning gaze fixation. In contrast, the subjects were asked to stare at the fixation spot (3 min of arc in diameter and 75 cd/m^2 in luminance) placed 25 min of arc above the central spot of the stimulus in the second series of Experiment III.

Observation time was practically unlimited. The difference in physical length between the test and referential intervals of the stimulus, determined after the perceived equality was achieved, was considered as the value of the illusion strength. For each set of an independent variable, each observer carried out at least 10 experimental runs on different days. One hundred and twenty presentations were included in a single experimental run, i.e., 40 values of an independent variable for 3 types of stimuli were taken randomly. A single experimental run usually lasted about half an hour. Ten trials went into each data point analysis, and the Student's coefficient $t_{0.95,10}$=2.262 was used to evaluate confidence intervals for the estimated means. In the data graphs, the error bars depict ± one standard error of the mean (SEM).

For the experimental data analysis, the procedures of the statistical and curve fitting toolboxes of SciLab (Scilab Group, INRIA ENPC) were used.

Subjects

University teachers and students were tested in the experiments. All observers were normally sighted or were wearing their usual optical corrections. Four subjects (NI, GD, VA, and LE) of six were naïve with respect to the goal of the study. The subjects gave their informed consent before taking part in the experiments which were performed in accordance with the ethical standards of the 1964 Helsinki Declaration.

EXPERIMENT I

Method

The aim of Experiment I was to determine quantitatively the strengths of the three illusions of extent as functions of the length of the wings (w), or the diagonal sides of the imaginary triangles. Therefore, the spatial parameters of the contextual objects (the wing length in Fig. 1A, the stripe length and position in Fig. 1B, the position of the pairs of the flanking spots in Fig. 1C) were given values that resulted in the same spatial positions for the end-points of the stripes, and the wings.

The length of the wings randomly varied from 0 to 20 min of arc in 0.5 min of arc steps. The internal angle of the wings (α) was fixed at 90º. The length of the referential part of the stimuli was 64 min of arc. Four subjects (UL, NI, GD, and VA) participated in Experiment I.

It was expected in Experiment I that for relatively short wings the experimental curves for different types of contextual flanks may coincide because Equations 6, 7, and 8 can be approximated by the linear functions, the slopes of which do not differ significantly. For longer wings, the linearity should be broken, and the curves should diverge, and the saturating or decreasing illusion strength should appear because of attenuation of influence of the more distant wing parts in the periphery of the attentional pooling windows.

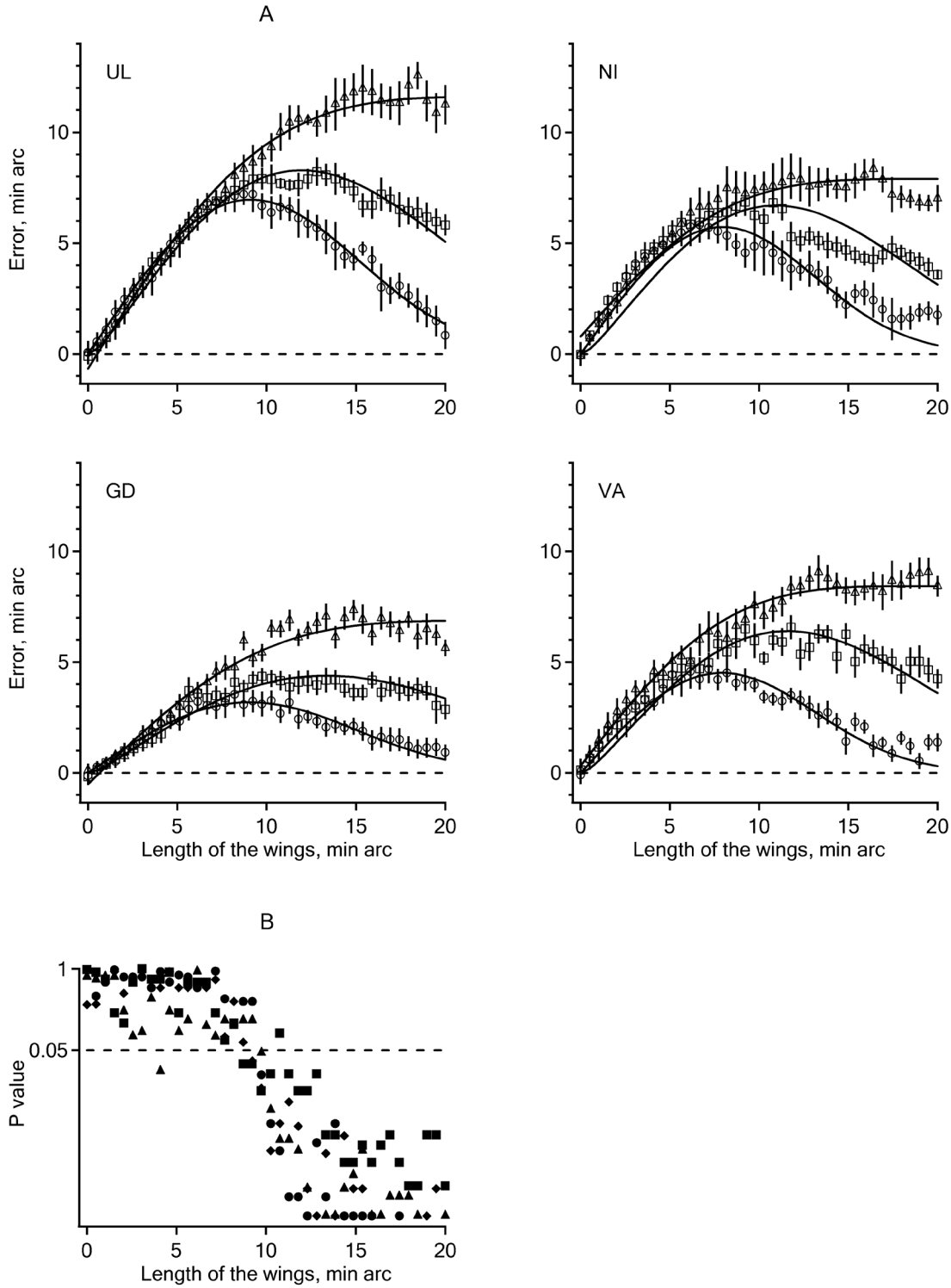

Fig. 4. Illusions of extent as a function of the length of the wings (*w*). Four subjects tested. (A) Triangles, squares, and circles represent the illusions induced by different contextual objects: the Müller-Lyer wings, stripes, and pairs of spots, respectively. Solid curves – the least squares fitting by Equations 11, 10, and 9, respectively. Length of the referential part of the stimuli, 64 min of arc; internal angle of the wings, 90º. Error bars, ± one standard error of the mean (SEM). (B) The results of the nonparametric Friedman ANOVA test applied to the experimental data shown in (A) for the four subjects: filled circles for UL, squares for NI, diamonds for GD, triangles for VA.

Results

For all subjects, the three functions obtained showed a monotonic growth of the illusions' magnitude with increase of the length of the wings from 0 to about 7 min of arc (Fig. 4A). For the length of the wings shorter than 9 min of arc, the Friedman ANOVA test indicated the absence of a significant difference between the data on different illusory figures (Fig. 4B).

The curves in Fig. 4A practically coincided for the wings shorter than 9 min of arc, but differed in higher length values: (a) the magnitude of the Brentano illusion (Fig. 4A, triangles) continued to grow with further increase of the length of the wings up to 15–20 min of arc; (b) the magnitude of the illusion with the flanking stripes (Fig. 4A, squares) gained its maximum near 10–12 min of arc and descended slightly afterwards; (c) the magnitude of the illusion with the flanking spots (Fig. 4A, circles) showed the maximum within the 6–9 min of arc interval and gradually decreased with the length of the wings. The results were qualitatively the same for all subjects, however, the absolute values of the illusion strength and the positions of its maximum values slightly differed.

Discussion

It is apparent in our experimental data that the simplest contextual flanks, the pairs of spots, exert their effect only when they are positioned sufficiently close to the end-spots of the stimulus (Fig. 4A, circles). The effect supports the suggestion that the local lateral interaction processes may take place within proximal surroundings of the stimulus terminators forming regions of the perceptual influence (or those of integration of the positional signals) which could correspond to the units with large receptive fields proposed by Morgan and coworkers (1990) or to the areas of centroid extraction, Ω defined in our modeling. Besides, a particular shape of curves (Fig. 4A, circles) can serve as a support for our assumption that the spatial profile of the area of integration may be related to the Gaussian function.

The functions of the illusion strength obtained in our experiments can be interpreted as some averaged biases which occur as a result of the summation of individual effects induced by three flanks with different retinal eccentricities, or, for simplicity, a result of an averaged individual effect multiplied by a certain coefficient of proportionality, *A*. The additivity of the perceptual influences of the individual flanks on the

Table I

The values of the fitting parameteres for data of Experiment I

Contextual flanks	Parameters	Subjects			
		UL	NI	GD	VA
Spots	A	2.5 ± 0.56	2.26 ± 1.04	1.26 ± 1.14	1.84 ± 1.38
	σ	6.25 ± 0.33	5.62 ± 0.59	6.02 ± 0.35	5.51 ± 0.46
	R^2	0.98	0.89	0.94	0.92
Stripes	A	1.69 ± 0.29	1.64 ± 0.65	1.07 ± 0.69	1.33 ± 0.79
	R^2	0.97	0.85	0.95	0.93
ML wings	A	3.66 ± 0.13	2.54 ± 0.21	2.22 ± 0.15	2.91 ± 0.15
	R^2	0.98	0.94	0.96	0.97

illusion strength has been confirmed in our earlier studies (Bulatov et al. 1997, Bulatov and Bertulis 2005b). When assuming that each flanking object in the stimulus contributes to the illusory effect with the same weight, the strength of the illusion should be four times greater (coefficient $A = 4$) than the bias caused by a single contextual flank: the lateral flanks yield two contributions, and the central one also provides two, because it changes the perceived length of both the referential and test intervals. Due to stimulus extent, all three stimulus parts cannot be foveated simultaneously, therefore, the contribution of each flank to the resulting illusion strength should be different, and the most probable values of the coefficient A should be found in the range from 1 to 4.

To test our computational model by using the simplest stimulus configuration, we fit the data shown in Fig. 4A (circles) with the function derived from Equation 6:

$$\Delta_{dd}(w,\alpha) = Aw\cos(0.5\alpha)\times \times \frac{2e^{-Bw^2\left[1+\cos(0.5\alpha)^2\right]}}{1+2e^{-Bw^2}} \quad (9)$$

where Δ_{dd} is the illusion strength; w is the wing length; α, the internal angle of the wings; A, coefficient of proportionality; $B = 1/2\sigma^2$, and determines the width of the Gaussian profile of the averaged area of centroid extraction, $\Omega_{averaged}$, which represents some weighted average of individual Ω sizes corresponding to the three stimulus terminators.

To fit the experimental data with functions comprising two free parameters A and B, the method of least squares with implementation of the optimized version of the Levenberg–Marquardt algorithm was used. A good resemblance between the computational and experimental data for all subjects was obtained (Table I).

Our experiments with the contextual objects formed by the line segments (triangles, and squares in Fig. 4A) show the quantitative characteristics of illusions similar to those obtained with the flanking spots when the relatively short wings were used. Conclusively, within the 0–9 min of arc interval, three different types of the flanks appended to the three-spot stimulus influence its perceived size, but the magnitude of the influence does not depend significantly on the shape of the appendages (Fig. 4B). However, the integral contribution of all parts of the contextual Müller-Lyer wings or vertical stripes yields the divergent segments of the experimental curves (squares, and triangles in Fig. 4A).

We have fitted the experimental data for the flanking vertical stripes with the function derived from Equation 7:

$$\Delta_{ds}(w,\alpha) = Aw\cos(0.5\alpha)\times \times \frac{e^{-\left[\frac{w\cos(0.5\alpha)}{\sigma}\right]^2} erf\left[\frac{w\sin(0.5\alpha)}{\sigma\sqrt{2}}\right]}{erf\left(\frac{s}{2\sigma\sqrt{2}}\right)+e^{-0.5\left[\frac{w\cos(0.5\alpha)}{\sigma}\right]^2} erf\left(\frac{w\sin(0.5\alpha)}{\sigma\sqrt{2}}\right)} \quad (10)$$

where s is the spot diameter (1.5 min of arc).

The data for the Müller-Lyer wings have been fitted with the function derived from Equation 8:

$$\Delta_{ml}(w,\alpha) = A\frac{\cos(0.5\alpha)\sigma\sqrt{2}}{1+\cos(0.5\alpha)^2}\times \times \frac{1-e^{-0.5\left(\frac{w}{\sigma}\right)^2\left[1+\cos(0.5\alpha)^2\right]}}{\sqrt{\pi}erf\left(\frac{w}{\sigma\sqrt{2}}\right)} \quad (11)$$

The σ values taken for calculations (10) and (11) are those obtained by fitting the data shown in Fig. 4A (circles) with function (9). A good correspondence between the computational and experimental data has been achieved for the flanking vertical stripes and the Müller-Lyer wings, like for the flanking pairs of spots (Table I). Since all three equations (9–11) are derived on the basis of the same principles of the automatic centroid extraction (see Methods), a success in fitting strongly supports the idea of a single neurophysiological mechanism underlying the illusions caused by the three different appendages.

Altogether, the curves obtained in Experiment I (Fig. 4A) show comparable perceptual distortions induced by different contextual objects forming the 90° internal angle of the wings within a certain range

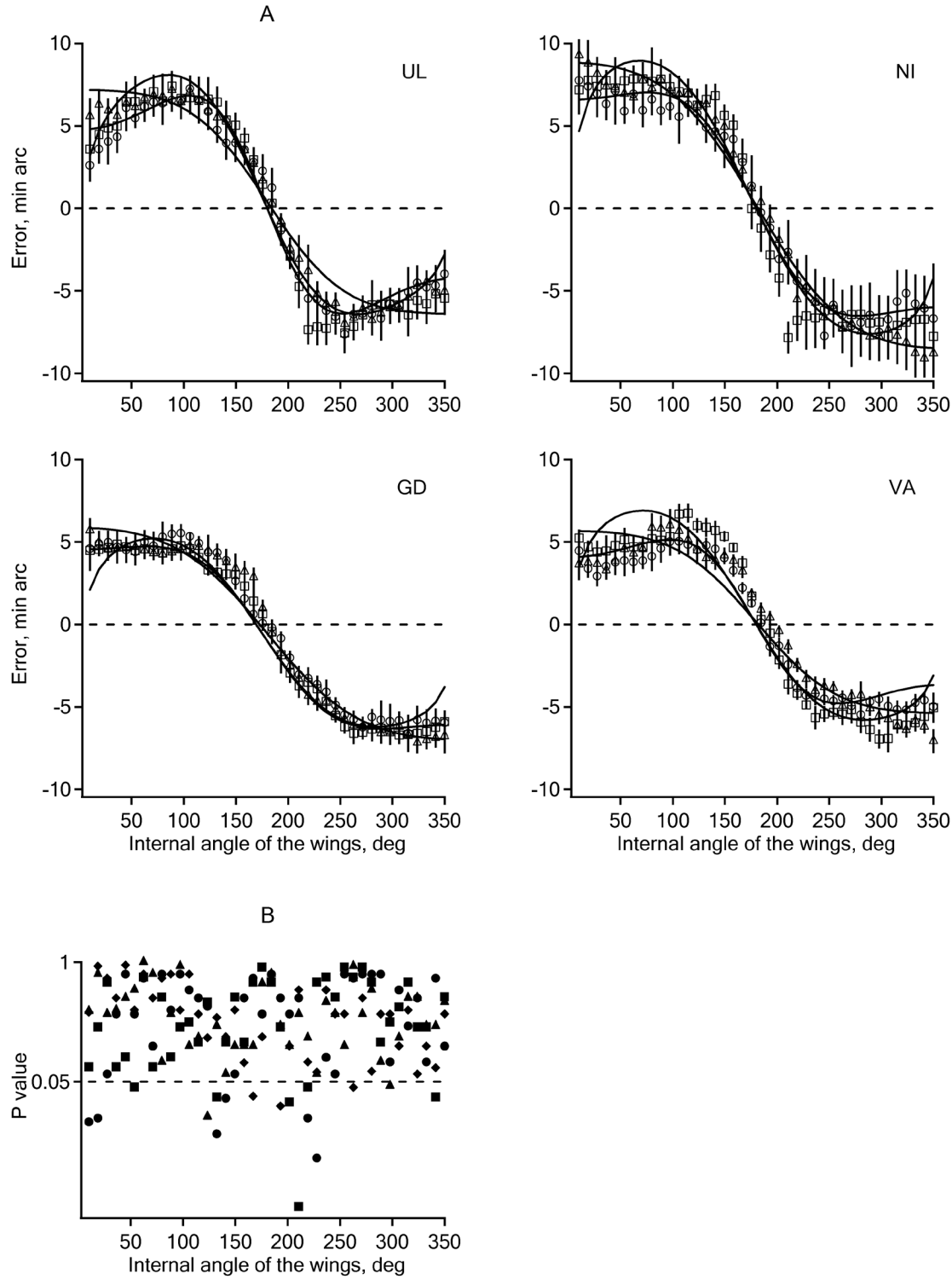

Fig. 5. Illusions of extent as a function of the internal angle of the wings (α) for four subjects. (A) Triangles, squares, and circles represent the illusions induced by different contextual objects: the Müller-Lyer wings, stripes, and pairs of spots, respectively. Solid curves – the least squares fitting by Equations 11, 10, and 9, respectively. Length of the referential part of the stimuli, 64 min of arc; length of the wings, 8 min of arc. Error bars, ± one standard error of the mean (SEM). (B) The results of the nonparametric Friedman ANOVA test applied to the experimental data shown in (A) for four subjects: filled circles for UL, squares for NI, diamonds for GD, triangles for VA.

Table II

The values of the fitting parameteres for data of Experiment II

Contextual flanks	Parameters	Subjects			
		UL	NI	GD	VA
Spots	A	3.61 ± 0.77	2.55 ± 0.67	1.57 ± 0.82	2.76 ± 1.52
	R^2	0.98	0.94	0.97	0.95
Stripes	A	2.16 ± 0.35	2.02 ± 0.46	1.01 ± 0.63	1.62 ± 0.71
	R^2	0.97	0.95	0.93	0.91
ML wings	A	1.72 ± 0.22	3.67 ± 0.3	2.61 ± 0.32	2.71 ± 0.48
	R^2	0.96	0.98	0.96	0.93

of their length. The length-matching distortions induced by the contextual objects with a fixed length of the wings but with varying internal angles were examined in Experiment II.

EXPERIMENT II

Method

In Experiment II, the internal angle of the contextual wings (α) was varied randomly from 10° to 350° in steps of 8.5°. The length of the referential part of the stimuli was 64 min of arc, and the length of the wings was fixed at 8 min of arc. The four subjects taking part in Experiment II also participated in Experiment I.

As it follows from the results of Experiment I, similar magnitudes of illusions for three different types of figures may be obtained because of relatively short wings used in the experiments.

According to properties of the functions (9–11) derived in our modeling, all curves in Experiment II were expected to have a shape similar to a cosine, which would be consistent with the results reported earlier by Davies and Spencer (1977). Nevertheless, some deviations from the cosine law ought to be present, because Equations 9–11 comprise not only the cosine function but some other sufficiently complex parts which depend, also, on the internal angle of the wings.

Results

Illusions as functions of the internal angle of the wings showed near symmetrical curves (similar to a cosine) with two parts comprising positive and negative values (Fig. 5A). When the internal angle approached 180°, the strength of illusions decreased to zero.

Though the length of the wings was relatively small (8 min of arc), the subjects had no difficulties in identifying the shapes of different contextual objects. Nevertheless, the subjects produced errors of about the same magnitude, irrespective of the perceived discrepancies in the structure of different flanks of the stimuli, e.g., when the wings were spread at the 120° angle, the absolute error value was about 7 min of arc for all three stimuli, one of which had appended wings of 8 min of arc long, while the other was flanked by vertical stripes about 14 min of arc high, and the third possessed pairs of spots only 1.5 min of arc in size. In the experiments, the error value and sign varied in a regular way with changes of the internal angle of the wings, but it did not depend noticeably on the contextual object type: three curves in Fig. 3A corresponding to the data for different stimuli practically coincided. The Friedman ANOVA test confirmed (with few exceptions) the absence of significant differences between the data for three different illusory figures (Fig. 5B).

Discussion

Fitting the data shown in Fig. 5A with functions (9), (10), and (11) provides a good correspondence between the computational and experimental results for all subjects (Table II: coefficient of determination R^2 in all cases is higher than 0.9). The σ values taken for fitting the data shown in Fig. 5A are those obtained by the fitting the data shown in Fig. 4A (circles) with function (9).

The results of Experiment II provide support for the explanations of the findings of Experiment I. Three curves for different illusory figures are similar in amplitude, and the shape of the curves resembles that of the fit. In other words, our computational model appeared to be powerful enough to predict both the shape of experimental curves as an approximate cosine, and all deviations from the cosine law within a certain range of internal angles of the wings.

Once again, a good correspondence between the computational and experimental data supports the idea about the same neurophysiological mechanism of automatic centroid extraction underlying the illusory percept caused by the three different appendages.

To examine the stimulus size influence on the illusion magnitude and to test further the validity of our model, Experiment III was conducted.

EXPERIMENT III

Method

We have used the Brentano figure formed of spots (Fig. 1C) because the figure consists of minimum number of identical elements (the spots), the positions of which are strictly determined within the stimulus pattern. In comparison with the other two figures used in previous experiments which comprised line segments, the figure formed of spots has a reduced number of foreign interfering factors.

The stimulus varied in size: the length of the referential part was 32, 64, and 96 min of arc. The strength of the illusion was measured as a function of the wing length, w which randomly varied from 0 to 20 min of arc in 0.5 min of arc steps. The internal angle of the wings, α was fixed at 90º. Three subjects (UL, ER, and LE) participated in the experiments, and one of them (UL) had participated also in Experiments I and II.

We performed two series of Experiment III with different viewing conditions. In the first series of Experiment III, the subjects were given no instructions concerning gaze fixation, and in the second series, the subjects were instructed to stare at the spot (3 min of arc in diameter and 75 cd/m^2 in luminance) which was placed 25 min of arc above the central spot of the stimulus. We have presumed that two different viewing conditions may cause different values of the averaged distance between the fovea center and the retinal positions of the three stimulus terminators. If one assumes that, in experiments without specified gaze fixation, the subjects focus their sight with the same probability at each stimulus terminator, the averaged distances could be estimated as $(2r/3 + 2r)/3$, where r is the length of the referential part. Then the values of the averaged distances would be about 28, 57, and 85 min of arc for the stimuli with the length of the referential part 32, 64, and 96 min of arc, respectively. In the second series of experiments, with a high probability that the subject's sight will be directed to the fixation spot, the averaged distances could be estimated as $[2\mathrm{sqrt}(r^2 + h^2) + h]/3$,where r is the length of the referential part, and h is the distance between the fixation and central spot of the stimulus, i.e. 25 min of arc. In this case, the averaged distances should be about 35, 54, and 74 min of arc, correspondingly.

Equation 9 predicts the illusion maximum and its position on the abscissa axis being proportional to the size of $\Omega_{\mathrm{averaged}}$ which, we suppose, is related to the averaged distance between the fovea center and the retinal positions of the three stimulus terminators. Therefore, we expected in the experiments to observe a shift of the position of the illusion maximum toward larger values of the wing length with increasing stimulus size for both viewing conditions – with gaze fixation and without it.

Also, we predicted the experimental results in which the position of the illusion maximum may be moved to larger values of the wing length for the small stimuli (with the referential part 32 min of arc) when the gaze fixation was present because the averaged distance between the stimulus terminators and the fovea center, according to our method of estimation, is about 22% larger than that in the experiments when gaze fixation was absent. For the larger stimuli, this shift of the position of the maximum may be less prominent because, in the stimulus with the referen-

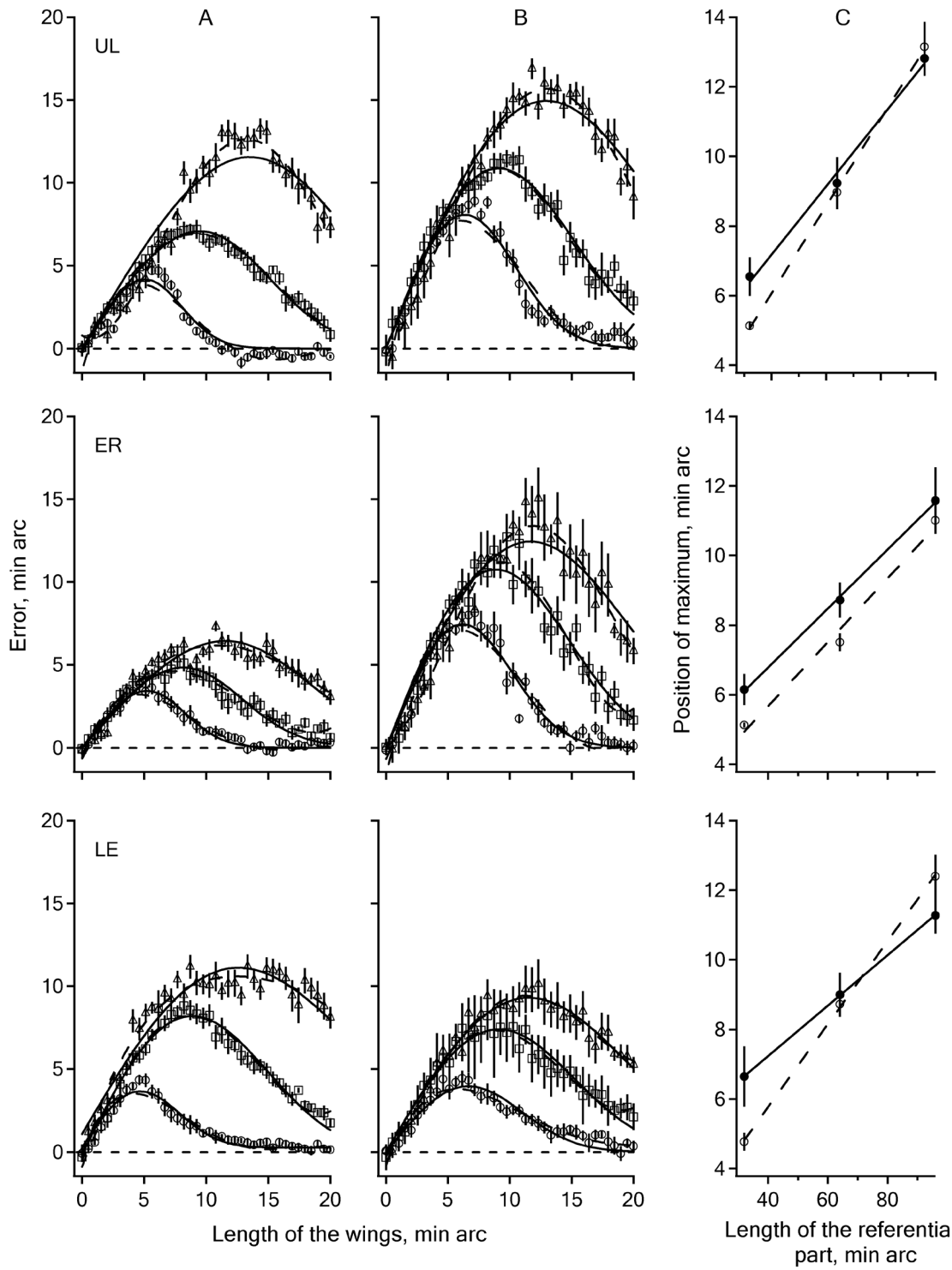

Fig. 6. Illusions of extent as a function of the length of the wings (w) for different stimulus sizes in the gaze fixating absence (A) and presence (B). Circles, squares, and triangles represent the data for the stimulus referential part different in length: 32, 64, and 96 min of arc, respectively. Dashed curves – polynomial fitting (5^{th} order). Solid curves – the least squares fitting by Equation 9. Error bars – ± one standard error of the mean (SEM). Subjects: UL, ER, and LE. (C) Dependences of the position of illusion maximum on the length of the referential part of the stimulus in the gaze fixating absence (dashed lines) and presence (solid lines).

Table III

The values of the fitting parameteres for data of Experiment III

RL	Subjects	Without gaze fixation			With gaze fixation		
		A	σ	R^2	A	σ	R^2
32	UL	3.2 ± 0.35	3.46 ± 0.19	0.93	4.09 ± 0.38	4.33 ± 0.35	0.95
	ER	2.23 ± 0.18	3.45 ± 0.14	0.96	3.89 ± 0.47	4.21 ± 0.29	0.95
	LE	2.46 ± 0.26	3.25 ± 0.17	0.93	1.93 ± 0.95	4.54 ± 0.58	0.92
64	UL	2.65 ± 0.13	6.3 ± 0.11	0.98	3.91 ± 0.38	6.24 ± 0.49	0.96
	ER	1.94 ± 0.18	5.26 ± 0.22	0.93	3.96 ± 0.65	6.09 ± 0.35	0.95
	LE	3.19 ± 0.21	6.14 ± 0.16	0.96	2.66 ± 1.34	6.24 ± 0.41	0.94
96	UL	3.51 ± 0.42	9.16 ± 0.47	0.93	3.81 ± 0.73	8.89 ± 0.36	0.97
	ER	1.96 ± 0.19	7.71 ± 0.26	0.93	3.51 ± 0.24	8.02 ± 0.65	0.94
	LE	2.69 ± 0.31	8.72 ± 0.39	0.93	3.14 ± 1.03	7.92 ± 0.35	0.94

(RL) the length of the referential part of the stimulus, min of arc

tial part 64 min of arc, the relative difference between the averaged distances is about −5%, and in the stimulus with the referential part 96 min of arc, the difference is about −14%.

Results

For both viewing conditions, the experimental curves obtained appear to be similar in shape (Fig. 6A and 6B), but the maximum values on the curves increase and the maxima positions on the abscissa axis shift toward the longer wings, when the lengths of the referential part of the stimulus increases.

For the quantitative estimation of positions of the maxima of illusions, the polynomial curves fitting (5^{th} order) were applied (Fig. 6A and 6B, dashed curves). The regression analysis of the dependence of the position of the illusion maximum on the length of the referential part of the stimulus revealed highly significant linear correspondence: correlation coefficients *r* were 0.98, 0.94, 0.95; slopes *b* 0.098 ± 0.008, 0.085 ± 0.003, 0.072 ± 0.001; intercepts *a* 3.26 ± 0.56, 3.39 ± 0.19, 4.34 ± 0.44 min of arc for subjects UL, ER, LE, respectively (Fig. 6C, dashed lines, gaze fixating absent); and correlation coefficients *r* were 0.96, 0.93, 0.97; slopes *b* 0.125 ± 0.003, 0.092 ± 0.01, 0.119 ± 0.002; intercepts *a* 1.07 ± 0.21, 2.0 ± 0.69, 1.0 ± 0.17 min of arc for subjects UL, ER, LE, respectively (Fig. 6C, solid lines, gaze fixating present).

When the gaze fixation was used, for the small stimuli with the referential part 32 min of arc, the shifts of the position of the illusion maximum to the larger values of the length of the wings (Fig. 6C) are statistically significant for all subjects (UL: t_{10}=7.831, P<0.001; ER: t_{10}=7.102, P<0.001; LE: t_{10}=6.562, P<0.001). For the larger stimuli with the referential parts 64 min of arc (t_{10}=1.059, ns; t_{10}=6.761, P<0.001; t_{10}=1.333, ns, for subjects UL, ER, and LE, respectively) and 96 min of arc (t_{10}=1.157, ns; t_{10}=1.817, ns; t_{10}=4.32, P<0.001, for subjects UL, ER, and LE, respectively), the shifts are much less reliable.

Discussion

The experimental data presented in Fig. 6A and 6B, which show in particular the shifts of the positions of the maxima on the curves toward the longer wings, support our assumption that the averaged area of centroid extraction, $\Omega_{averaged}$ increases with the length of the referential part of the stimulus. The increase can be related to an enlargement of the individual Ω's due to changes of the retinal eccentricities of the corresponding stimulus terminators. In the viewing conditions with the gaze fixation, only the positions of the lateral terminators vary relatively to the fixation spot with the changes of the length of the referential part of the stimulus, and the position of the central spot does not change. Consequently, the contribution of the central Ω to $\Omega_{averaged}$ is relatively small and invariable, and the size of $\Omega_{averaged}$ ought to be determined mainly by the lateral Ω's. On the contrary, in the viewing conditions without gaze fixation, the positions of all terminators are not fixed relatively to the fovea center, and contributions of all Ω's to $\Omega_{averaged}$ vary individually. Therefore, for the same stimulus size, $\Omega_{averaged}$ may be not the same in two viewing conditions. Indeed, the significant shift of the position of the illusion maximum when viewing conditions change (Fig. 6C, the stimuli with the referential part 32 min of arc) confirms the assumption on the $\Omega_{averaged}$ differences and demonstrates importance of the gaze fixating in the experiments.

Fitting the curves with function (9) showed a good correspondence between the computational and experimental data for all subjects (Fig. 6A and 6B, solid curves, and Table III). The fitting parameters provide quantitative estimation of widths of $\Omega_{averaged}$ as the spreads of Gaussians with two standard deviations σ on either side of the mean. The width of $\Omega_{averaged}$ increases with the stimulus size, and the regression analysis reveals highly significant linear correspondence for both viewing conditions, with gaze fixation (correlation coefficients r were 0.97, 0.96, 0.94; slopes b 0.31 ± 0.03, 0.26 ± 0.027, 0.23 ± 0.031; intercepts a 4.79 ± 1.82, 6.25 ± 1.89, 9.11 ± 2.21 min of arc for subjects UL, ER, LE, respectively), and without it (correlation coefficients r were 0.98, 0.98, 0.93; slopes b 0.35 ± 0.04, 0.27 ± 0.034, 0.34 ± 0.029; intercepts a 2.43 ± 0.72, 4.81 ± 0.83, 2.33 ± 1.43 min of arc for subjects UL, ER, LE, respectively).

The estimated size of $\Omega_{averaged}$ for the negligible small stimulus (the value of averaged intercept of the linear regressions for all subjects) is about 4.9 min of arc. The size of $\Omega_{averaged}$ for the stimulus with the length of the referential part 96 min of arc is about 33.6 min of arc. These results are consistent with the psychophysical data on the attentional resolution: the size of the "spotlight of attention" increases with the retinal eccentricity from about 3–5 min of arc at the fovea center to about 25–35 min of arc at 1.3º eccentricity (Nakayama and Mackaben 1989, Intriligator and Cavanagh 2001).

GENERAL DISCUSSION

In our communication, we present a detailed mathematical description of a possible physiological mechanism of centroid extraction and use it in explanations of origin of the illusions of extent. Our computational approach assumes certain integration procedures in the visual pathways – a weighted spatial pooling of the neural excitations evoked by the stimulus terminators and flanks, and the convolution of two profiles, those of the attentional pooling and of the receptive fields of certain summation units. These procedures provide information about the position of the pooling centroid. The visual system identifies the position of the pooling centroid with the position of the stimulus terminator, and the latter appears to be shifted perceptually. The perceptual shifts of the three stimulus terminators lead to misestimating of the spatial intervals flanked by the contextual objects.

The explanation of illusion origin based on the idea of the automatic centroid extraction has been developing in a number of previous studies (Virsu 1971, Coren 1986, Morgan et al. 1990, DeLucia et al. 1994, Searleman et al. 2005, Seizova-Cajic and Gillam 2006), but the present approach differs slightly from others in definition of centroid considered. We believe that the visual system does not possess the mechanism for extraction of an exact, strictly in a physical sense, centroid of the lightness distribution of a cluster of neighboring stimulus elements. Instead, the visual system uses information about the position of the "physiological" centroid of the neural excitatory relief modulated by the weighting profile of the attentional window. The "physical" and "physiological" centroids practically coincide for small objects (in comparison with the width of the attentional window), but they can

markedly differ for larger objects because of failure of additivity of centroids corresponding to separate parts of the objects. Therefore, objects composed of several different parts cannot to be perceived simply as "located at the centroid of the individually measured positions of their separate parts" (Morgan et al. 1990, p. 1800).

Some properties of the attentional window used in our modeling can be related to those of the "attentive interactive fields" proposed by Pressey and Pressey (1992) in their integrative field theory, e.g., both the centers of the circular "interactive fields" and the attentional windows are located at the stimulus terminators; the weighting profiles of the fields and the windows are described by the functions which gradually decrease in periphery. However, the interactive field is considered "as a logical-mathematical construct that refers to a field of probability" (Pressey and Pressey 1992, p. 423) whose size and weighting profile parameters depend heavily on the spatial structure of the stimulus contextual flanks. In our case, for all types of the contextual flanks, we assume the same structure of the attentional windows (circular Gaussians) the sizes of which depend only on their retinal eccentricity. Moreover, the positioning of the attentional windows precisely at the stimulus terminators is not crucial in our modeling. Varying the relative positions of the attentional windows yields only slight changes of the functional dependencies of the illusion magnitude which may be encountered in the experimental results as the trial-to-trial variability, e.g., a certain asymmetry of the curves for the internal angle of the wings, and the changes of the maximum value and its position on the curves for the wing length.

We have tested our model by the functional dependencies of perceptual distortions established in the psychophysical experiments, and the modeling functions replicated properly all variations of the illusion strength obtained for different types of stimuli, for all subjects, and in different viewing conditions. Results of fitting of experimental data yielded physiologically substantiated parameters of the mechanism underlying the effect of illusion: the values of width of the area of centroid extraction, and the coefficient of proportionality A. However, some sources of possible inaccuracies are apparent in our calculations. First, it is the same type of the weighting profiles (Gaussian) of the attentional window and summation units. For instance, the Gaussian profile of the attentional window may be not applicable for modeling the effects of reversed Müller-Lyer illusion which were observed in the experiments (Worrall and Firth 1974, Restle and Decker 1977) with the stimulus configurations possessing a gap between the wings and the shaft. With our stimuli, the effect of reversed illusion was not established because the absence of the shafts or their segments (which may be considered as additional wings with zero internal angle). However, we believe that the reversed illusion effect can be modeled properly by using LoG (or DoG) function (Fig. 3B, right). Also, we have taken the same width of the attentional window and summation units because the actual ratio of sizes is not known. Variations of the ratio of the widths could cause, by our estimations, changes of calculated sizes of Ω_{averaged} in the range of about 1.5 times with coherent values of the coefficient A which should remain in the range from 1 to 4.

The second source of inaccuracy is related both to Formula 5, which only approximately reflects the procedure of centroid extraction, and to the simplified description of the relief of neural excitations evoked by the stimulus parts. According to our computational evaluations, the goodness of fitting the results of the exact root-finding by Formula 5 gradually diminishes with increase of the ratio of masses of the distractor and target. Also, changes in the relief of the neural excitations (e.g., blurring) caused by the filtering at early stages of visual processing can slightly increase the values of calculated sizes of Ω_{averaged}.

And the third source of inaccuracy in our modeling is due to significant uncertainty in estimating of interrelations between the stimulus size and actual retinal eccentricities of the stimulus terminators. This factor dramatically limits our possibility to evaluate precisely the parameters of increase of the area of centroid extraction with its eccentricity in the visual field.

Despite the limitations mentioned above, our computational approach offers a sufficiently simple way of the analytical description of the illusion dependencies on various parameters of the stimuli used. The equations derived may be easily tested by varying the other stimulus parameters, e.g., luminance contrast, size, number, and relative positions of elements in the flanking objects. Also, the equations can be modified for application to untested patterns. This is a distinctive property of our approach in comparison with ear-

lier qualitative theories on the illusions' origin (Gregory 1963, 1968, Gillam 1998) and with more recent explanation concerning the observer's sensitivity to statistical regularities within the environment (Howe and Purves 2005).

Our theoretical propositions concerning the genesis of illusions are consistent with theories based on the effects of spatial frequency filtering in early visual processing (Coren and Girgus 1978, Bulatov et al. 1997, Fermüller and Malm 2004, Bulatov and Bertulis 2005a) because the procedures of convolution and the attentional pooling in our modeling can be considered as equivalent to consequent stages of the low-pass or band-pass spatial filtering. The particular properties of the filtering at different levels of the visual system are beyond the limits of the present communication. A combined model of perceptual distortions can be taken as an object of interest for subsequent studies.

The biological significance of the mechanism of the automatic centroid extraction is that it enables fast and reliable estimation of location of the visual object as a whole independently of its size and shape complexity. The resulting advantages of the mechanism considerably outweigh the losses (which manifest themselves in the form of illusions) caused by the side-effects of the processes of local integration of the positional signals.

CONCLUSIONS

In the present study, we have developed a computational model of the automatic centroid extraction based on the processes of local integration of excitatory profiles in the visual pathways. Predictions of the model have been compared with the results of the psychophysical testing of three geometric illusions of extent with different contextual flanks. Good correspondences between the computational and experimental data obtained have provided evidence that the side-effects of indirect positional coding *via* centroids are powerful enough to be considered as one of the main causes for the illusions of extent investigated. We believe that the computational approach proposed in our modeling can be fruitful in examining the wide range of illusory patterns of various spatial structures.

ACKNOWLEDGEMENT

This work was supported by the Scientific Fund of Kaunas University of Medicine.

REFERENCES

Baldwin JM (1895) The effect of size-contrast upon judgements of position in the retinal field. Psychol Rev 2: 244–259.

Bertulis A, Bulatov A, Bielevicius A (2008) Influence of distracter on perceived stimulus length and angle size. Psichologija (Vilnius) 38: 29–39.

Bettencourt KC, Somers DC (2009) Effects of target enhancement and distractor suppression on multiple object tracking capacity. J Vision 7: 1–11.

Brigell M, Uhlarik J, Goldhorn P (1977) Contextual influences on judgements of linear extent. J Exp Psychol Hum Percept Perform 3: 105–118.

Bulatov A, Bertulis A (2005a) Superimposition of illusory patterns with contrast variations. Acta Neurobiol Exp (Wars) 65: 51–60.

Bulatov A, Bertulis A (2005b) Distracting effect in length matching. Acta Neurobiol Exp (Wars) 65: 265–269.

Bulatov A, Bertulis A, Mickiene L (1997) Geometrical illusions: study and modelling. Biol Cybern 77: 395–406.

Cavanagh P, Alvarez GA (2005) Tracking multiple targets with multifocal attention. Trends Cogn Sci 9: 349–354.

Chiang C (1968) A new theory to explain geometrical illusions produced by crossing lines. Percept Psychophys 3: 174–176.

Coren S, Hoening P (1972) Effect of non-target stimuli upon length of voluntary saccades. Percept Mot Skills 34: 499–508.

Coren S, Girgus JS (1978) Seeing is Deceiving: The Psychology of Visual Illusions. Lawrence Erlbaum Associates, Hillsdale, NJ.

Coren S (1986) An efferent component in the visual perception of direction and extent. Physiol Rev 93: 391–410.

Davies TN, Spencer J (1977) An explanation for the Müller-Lyer illusion. Percept Mot Skills 45: 219–224.

Day RH (1972) Visual spatial illusions: A general explanation. Science 175: 1335–1340.

DeLucia PR, Longmire SP, Kennish J (1994) Diamond-winged variants of the Muller-Lyer figure: A test of Virsu's (1971) centroid theory. Percept Psychophys 55: 287–295.

Desimone R, Duncan J (1995) Neural mechanisms of selective visual attention. Ann Rev Neurosci 18: 193–222.

Earle DC, Maskell S (1993) Fraser cords and reversal of the café wall illusion. Perception 22: 383–390.

Fermüller C, Malm H (2004) Uncertainty in visual processes predicts geometrical optical illusions. Vision Res 44: 727–749.

Festinger L, White CW, Allyn MR (1968) Eye movements and decrement in the Müller-Lyer illusion. Percept Psychophys 3: 376–382.

Fink GR, Marshall JC, Weiss PH, Toni I, Zilles K (2002) Task instructions influence the cognitive strategies involved in line bisection judgments: evidence from modulated neural mechanisms revealed by fMRI. Neuropsychologia 40: 119–130.

Gandhi SP, Heeger DJ, Boynton GM (1999) Spatial attention affects brain activity in human primary visual cortex. Proc Natl Acad Sci U S A 16: 3314–3319.

Gillam B (1980) Geometrical illusions. Sci Am 242: 102–111.

Gillam B (1998) Illusions at century's end. In: Perception and Cognition at Century's End (Hochberg J, Ed.). Academic Press, London, UK, p. 95–136.

Ginsburg AP (1984) Visual form perception based on biological filtering. In: Sensory Experience, Adaptation and Perception (Spilman L, Wooten GR, Eds.). Lawrence Erlbaum Associates, Hillsdale, NJ, p. 53–72.

Glass L (1970) Effect of blurring on perception of a simple geometrical pattern. Nature 228: 1341–1342.

Gregory RL (1963) Distortion of visual space as inappropriate constancy scaling. Nature 119: 678.

Gregory RL (1968) Visual illusions. Sci Am 219: 66–67.

Howe CQ, Purves D (2005) The Müller-Lyer illusion explained by the statistics of image-source relationships. Proc Natl Acad Sci U S A 102: 1234–1239.

Intriligator J, Cavanagh P (2001) The spatial resolution of visual attention. Cogn Psychol 43: 171–216.

Kaufman L, Richards W (1969) Spontaneous fixation tendencies for visual forms. Percept Psychophys 5: 85–88.

Kelly SP, Gomez-Ramirez M, Foxe JJ (2008) Spatial attention modulates initial afferent activity in human primary visual cortex. Cereb Cortex 18: 2629–2636.

Levi DM, Klein SA, Aitsebaomo AP (1985) Vernier acuity, crowding, and cortical magnification. Vision Res 25: 963–977.

Mack A, Heuer F, Villardi K, Chambers D (1985) The dissociation of position and extent in Müller-Lyer figures. Percept Psychophys 37: 335–344.

McLaughlin SC, De Sisto MJ, Kelley MJ (1969) Comment on "Eye movement and decrement in the Müller-Lyer illusion". Percept Psychophys 5: 288.

Morgan MJ, Aiba TS (1985) Vernier acuity predicted from changes in the light distribution of the retinal image. Spat Vis 1: 151–161.

Morgan MJ (1999) The Poggendorf illusion: a bias in the estimation of the orientation of virtual lines by second-stage filters. Vision Res 39: 2361–2380.

Morgan MJ, Casco C (1990) Spatial filtering and spatial primitives in early vision: An explanation of the Zöllner-Judd class of geometrical illusions. Proc Biol Sci 242: 1–10.

Morgan MJ, Hole GJ, Glennerster A (1990) Biases and sensitivities in geometrical illusions. Vision Res 30: 1793–1810.

Morinaga S (1941) Some considerations on the explanation of the Muller-Lyer illusion. Japanese Journal of Psychology 16: 26–39.

Müller-Lyer FC (1896) Zur Lehre von den optischen Täuschungen über Kontrast und Konfluxion. Zeitschrift für Psychologie 9: 1–16.

Nakayama K, Mackaben M (1989) Sustained and transient components of focal visual attention. Vis Res 29: 1631–1647.

Posner MI, Petersen SE (1990) The attention system of the human brain. Ann Rev Neurosci 13: 25–42.

Pressey AW, Pressey CA (1992) Attentive fields are related to focal and contextual features: A study of Müller-Lyer distortions. Percept Psychophys 51: 423–436.

Restle F, Decker J (1977) Size of the Müller-Lyer illusion as a function of its dimensions: Theory and data. Percept Psychophys 21: 489–503.

Robinson DL, Petersen SE (1992) The pulvinar and visual salience. Trends Neurosci 15: 127–132.

Sagi D, Julesz B (1986) Enhanced detection in the aperture of focal attention during simple shape discrimination tasks. Nature 321: 693–695.

Searleman A, Porac C, Brzuszkiewicz L (2003) Changing the strength of the horizontal/vertical illusion by altering the placement of the functional fovea. Poster presented at the Eastern Psychological Association, Baltimore, MD.

Searleman A, Porac C, Sherman M (2004) Manipulating the strength of the Ponzo illusion by controlling the position of the functional fovea. Poster presented at the Eastern Psychological Association, Washington, DC.

Searleman A, Porac C, Dafoe C, Hetzel B (2005) Altering Mueller–Lyer illusion magnitude using figural additions at the wing–shaft intersections. Am J Psychol 118: 619–637.

Seizova-Cajic T, Gillam B (2006) Biases in judgments of separation and orientation elements belonging to different clusters. Vision Res 46: 2525–2534.

Sierra-Vázquez V, Serano-Pedraza I (2007) Single-band amplitude demodulation of Müller-Lyer illusion images. Span J Psychol 10: 3–19.

Solomon JA, Felisberti FM, Morgan MJ (2004) Crowding and the tilt illusion: Toward a unified account. J Vision 4: 500–508.

Somers DC, Dale AM, Seiffert AE, Tootell RBH (1999) Functional MRI reveals spatially specific attentional modulation in human primary visual cortex. Neurobiology 96: 1663–1668.

Tausch R (1954) Optische Taüschungen als artifizielle Effekte der Gestaltungs-prozesse von Grössen und Formenkonstanz in der natürlichen Raumwahrnehmung. Psychologische Forschung 24: 299–348.

Toet A, Levi DM (1992) The two-dimensional shape of spatial interaction zones in the parafovea. Vision Res 32: 1349–1357.

Virsu V (1971) Tendencies to eye movement, and misperception of curvature, direction, and length. Percept Psychophys 9: 65–72.

Ward LM, Coren S (1976) The effect of optically induced blur on the magnitude of the Mueller-Lyer illusion. Bull Psychonom Soc 7: 483–484.

Watt RJ, Morgan MJ (1983) The recognition and representation of edge blur: Evidence for spatial primitives in vision. Vision Res 23: 1465–1477.

Welch RB, Post RB, Lum W, Prinzmetal W (2004) The relationship between perceived length and egocentric location in Muller-Lyer figures with one versus two chevrons. Percept Psychophys 66: 1095–1104.

Westheimer G, McKee SP (1977) Spatial configurations for visual hyperacuity. Vision Res 17: 941–947.

Worrall N, Firth D (1974) The components of the standard and reverse Müller-Lyer illusions. Quart J Exp Psychol 26: 342–354.

Yarbus AL (1967) Eye Movements and Vision. Plenum Press, NY.